Chemistry–A European Journal
Research Article
doi.org/10.1002/chem.202403462
Chemistry Europe
European Chemical Societies Publishing
www.chemeurj.org

A Nanosized {Ni^{II}_{18}} Cluster with a 'Flying Saucer' Topology Exhibiting Slow Relaxation of Magnetisation Phenomena at Both 15 K and 1.3 K

Angeliki A. Athanasopoulou,[a] Parisa Abbasi,[a] Dimitris I. Alexandropoulos,[a, b] John J. Hayward,[a] Christine M. Beavers,[c] Simon J. Teat,[c] Wolfgang Wernsdorfer,[d, e, f] Júlia Mayans,[g] Albert Escuer,[g] Melanie Pilkington,*[a] and Theocharis C. Stamatatos*[a, b]

A high-nuclearity {Ni_{18}} complex (**1**) with a unique 'flying saucer' motif has been prepared from the organic chelate, α-methyl-2-pyridine-methanol (mpmH), in conjunction with bridging azido (N_3^-) and peroxido (O_2^{2-}) ligands. Magnetic susceptibility measurements revealed the presence of both ferro- and antiferromagnetic exchange interactions between the metal centres in **1**, and the stabilization of spin states with appreciable *S* values at two different temperature regimes. The end-on bridging azido and alkoxido groups are in all likelihood the ferromagnetic mediators, while the η^3:η^3:μ_6-bridging peroxides most likely promote the antiparallel alignment of the metals' spin vectors, yielding an overall non-zero spin ground state for the centrosymmetric compound **1**. Furthermore, the {Ni_{18}} nanosized cluster behaves as a single-molecule magnet, exhibiting magnetic hysteresis at low temperatures and two relaxation processes at 15 K and 1.3 K, a very rare phenomenon in polynuclear magnetic *3d*-metal clusters.

Introduction

Single-molecule magnets (SMMs) based on polynuclear metal complexes are 0-D systems displaying slow relaxation of magnetization as a result of the combination of a large ground state spin, *S*, together with a significant magnetic anisotropy of the Ising, or easy axis type, the latter reflected in the negative zero-field splitting parameter, *D*.[1] This combination leads to a significant barrier to magnetization reversal, whose upper limit (*U*) is given by $S^2|D|$ or $(S^2 - \frac{1}{4})|D|$ for integer and half-integer values of *S*, respectively. Experimentally, SMMs exhibit super-paramagnet-like properties that are characterized by the presence of a frequency-dependence to the out-of-phase component of the *ac* magnetic susceptibility, as well as magnetic hysteresis.[2] Although these properties can be ascribed to classical magnets, SMMs are considered to be true 'mesoscale' particles that straddle the boundary between the classical and quantum world, as evidenced by their ability to undergo quantum tunneling of their magnetization (QTM).[3]

Since the discovery of the first SMM $[Mn_{12}O_{12}(O_2CMe)_{16}(H_2O)_4]$,[4] the largest class of SMMs comprises paramagnetic *3d*-transition metal ions with cluster topologies.[5] These polymetallic species are not only attractive from a structural perspective (high-symmetry, aesthetically pleasing topologies and architectures),[6] but also represent a molecular 'bottom-up' approach for the assembly of nanoscale magnets, that lend themselves to potential applications in high-density information storage, molecular spintronics and as qubits for

[a] *Dr. A. A. Athanasopoulou, Dr. P. Abbasi, Dr. D. I. Alexandropoulos, Dr. J. J. Hayward, Prof. Dr. M. Pilkington, Prof. Dr. T. C. Stamatatos*
Department of Chemistry
Brock University
1812 Sir Isaac Brock Way
L2S 3A1 St. Catharines, Ontario, Canada
E-mail: mpilkington@brocku.ca

[b] *Dr. D. I. Alexandropoulos, Prof. Dr. T. C. Stamatatos*
Department of Chemistry
University of Patras
Patras 26504, Greece
E-mail: thstama@upatras.gr

[c] *Dr. C. M. Beavers, Dr. S. J. Teat*
Advanced Light Source
Lawrence Berkeley National Laboratory
1 Cyclotron Road, Berkeley,CA 94720, USA

[d] *Prof. Dr. W. Wernsdorfer*
Institut Néel, CNRS & Université Grenoble Alpes
BP 166, 25 avenue des Martyrs 38042 Grenoble Cedex 9, France

[e] *Prof. Dr. W. Wernsdorfer*
Physikalisches Institut, Karlsruhe Institute of Technology (KIT)
Wolfgang-Gaede-Str. 1, D-76131 Karlsruhe, Germany

[f] *Prof. Dr. W. Wernsdorfer*
Institut für Nanotechnologie, Karlsruhe Institute of Technology (KIT)
Hermann-von-Helmholtz-Platz 1, D-76344 Eggenstein-Leopoldshafen, Germany

[g] *Dr. J. Mayans, Prof. Dr. A. Escuer*
Departament de Quimica Inorganica i Organica and Institut de Nanociencia i Nanotecnologia (IN2UB), Universitat de Barcelona Marti i Franques 1-11, 08028 Barcelona, Spain

Supporting information for this article is available on the WWW under https://doi.org/10.1002/chem.202403462Supporting information for this article is available on the WWW under https://doi.org/10.1002/chem.202403462

quantum computation.[7] Mn^{III} clusters have been at the forefront of this field for many years since the Jahn-Teller distortion associated with these ions in O_h symmetry provides significant molecular anisotropy, as reflected in the cluster, $[Mn^{III}_6O_2(Et\text{-}sao)_6(O_2CPh(Me)_2)_2(EtOH)_6]$ (where Et-saoH$_2$ = 2-hydroxyphenylpropanone oxime), which possesses the largest anisotropy barrier for any *3d*-metal cluster based SMM to date, with an effective energy barrier, U_{eff}, of 86.4 K.[8] Although this hexametallic family of clusters has been expanded to include other paramagnetic *3d*-metal ions, small-to-negligible *D* values have afforded systems with much smaller U_{eff}.[9]

The field of SMMs changed in 2003 when Ishikawa *et al.* reported a mononuclear, double-decker Tb^{III} phthalocyanine complex with a large U_{eff} of 230 K.[10] Since then, a new era has emerged where research efforts are focused on the enhancement of molecular anisotropy via the synthesis of *4f*-metal complexes with small nuclearities and large, unquenched orbital angular momenta.[11] In contrast to the *3d*-metal clusters, the coupling between neighbouring Ln^{III} ions in these complexes is negligible due to the efficient shielding of the *4f* electrons by the filled *5s* and *5p* orbitals, resulting in slow relaxation of magnetization that is mainly attributed to single-ion effects.[12]

For both nanosized *3d*- and *4f*-metal based clusters, the choice of organic chelating ligand as well as the 'blend' of organic/inorganic ligands is of vital importance. Restricting our discussion to the former class of molecular nanomagnets, the bridging organic and/or inorganic ligands should be capable of: i) linking many *3d*-metal centres, permitting the self-assembly of large polymetallic clusters, and ii) facilitating the propagation of ferromagnetic exchange interactions. To date, many such families of ligands have been developed affording beautiful clusters with large *S* values, but only moderate energy barriers when compared to their *4f* counterparts.

2-(hydroxymethyl)pyridine (hmpH) belongs to the family of pyridyl alchohol ligands that have played an important role in the discovery of large *3d*-metal clusters, high-spin molecules and SMMs (Scheme 1).[13] In addition, the N_3^- ion bridging in a 1,1- or end-on-fashion is usually a ferromagnetic mediator for a wide range of acute and slightly obtuse M–N–M (M = metal) angles, and is thus considered to be an excellent co-ligand for the synthesis of high-spin molecules.[14] Furthermore, the employment of the hmp^- anion in Ni^{II} coordination chemistry has afforded many complexes, the majority of which are ferromagnetic $\{Ni_4\}$ cubanes, several of which display SMM properties.[15] Nevertheless, SMMs containing Ni^{II} are far less common than their Mn^{III} counterparts, despite the fact that mononuclear octahedral Ni^{II} complexes can have $|D| > 10\ cm^{-1}$.[16]

We have recently initiated a new program of research aimed at the development of small, potentially chiral chelating ligands for the discovery of metal clusters with unprecedented structural motifs and novel magnetic and/or electronic properties. In this context, our target ligand, α-methyl-2-pyridinemethanol (mpmH, Scheme 1), previously unexplored in the field of *3d*-cluster chemistry, possesses similar coordination features to hmpH, but subtly differs in its steric and electronic nature. Previous studies by this group involving selective *3d*-ions with both chiral and racemic forms of mpmH to date includes: (i) the investigation of chiral-mpmH with Co^{II} which afforded two homochiral mixed valence complexes $[Co^{II}Co^{III}_2(mpm)_6](ClO_4)_2$ and $[Co^{II}_2Co^{III}_2(OMe)_2(mpm)_4(NO_3)_4]$ with linear and tetranuclear cores, respectively, and non-SMM behaviour;[17] (ii) the cluster chemistry of *rac*-mpmH with Mn^{II} which yielded a mixed-valence nanosized $\{Mn_{31}\}$ cluster exhibiting SMM properties with a large energy barrier of 60 K,[18] and (iii) the employment of chiral and *rac*-mpmH together with suitable Ni^{II} salts which led to a chiral $\{Ni_4\}$ cubane,[19] and a $\{Ni_8\}$ cluster with a trapezoidal prismatic topology,[20] both of which did not display any SMM behaviour. We report herein the synthesis, structural and magnetic properties of a large nanosized $\{Ni_{18}\}$ cluster (**1**), with a unique 'flying saucer' topology and rare SMM behavior for a Ni^{II}-based coordination compound.

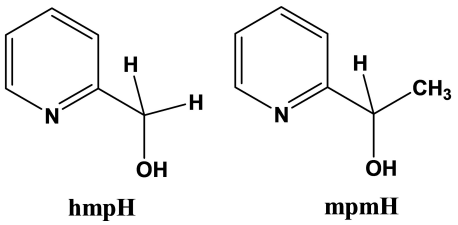

Scheme 1. Molecular structures of the ligands hmpH and mpmH.

Experimental Methods

Synthesis

For the synthesis of complex **1**, all reactions were performed under aerobic conditions using chemicals and solvents as received. The ligand *rac*-mpmH was prepared as described elsewhere,[21] and was characterized with CHN elemental analyses, and IR, ESI-MS and NMR spectroscopy to confirm its identity and purity (Figures S1–S3). Although no such behavior was observed during the present work, azide salts are potentially explosive and its compounds should be synthesized and used in small quantities, and treated with utmost care at all times.

$[Ni_{18}(O_2)_4(OH)_{3.62}(N_3)_{22.02}(NO_3)_{1.18}$(*rac*-mpm)$_{1.18}(MeCN)_{12}]$ (1). To a stirred, colorless solution of *rac*-mpmH (0.02 g, 0.20 mmol) and NEt_3 (28 μL, 0.20 mmol) in MeCN (15 mL) was added solid $Ni(NO_3)_2 \cdot 6H_2O$ (0.12 g, 0.40 mmol). The resulting bluish solution was stirred for 5 min, followed by the addition of an aqueous solution of H_2O_2 (6 μL, 0.06 mmol) and solid NaN_3 (0.05 g, 0.70 mmol). The obtained pale green suspension was refluxed for 30 min, during which time the solids dissolved and the color of the solution turned to deep green. The resulting solution was cooled, filtered, and left for slow evaporation at room temperature. After a period of two months, X-ray quality green block-like crystals of $\mathbf{1} \cdot 0.5MeCN \cdot 1.42H_2O$ were collected by filtration, washed with cold MeCN (2 x 2 mL) and dried in air. The yield was 5% (3.5 mg). Elemental analysis (%) calcd for $\mathbf{1} \cdot 2H_2O$: C 13.28, H 1.87, N 38.60; found: C 13.49, H 2.16, N 38.22. Selected IR data (ATR): ν = 3338 (mb), 2082 (s, ν(N-N)), 1581 (s), 1527 (s), 1437 (s), 1401 (m), 1348 (mb), 1177 (m), 1146 (m), 1110 (m), 978 (m), 922 (m), 891 (m, ν(O–O)), 848 (m), 820 (m), 755 (m), 660 (m), 616 (m), 587 (m), 537 (m), 460 (w), 431 (m).

X-ray Crystallography

A green block-like crystal (0.100×0.050×0.030 mm^3) of **1**·0.5MeCN·1.42H_2O was mounted on a MiTeGen kapton loop in the 100(2) K nitrogen cold stream provided by an Oxford Cryosystems Cryostream 700 Plus apparatus. The crystal was transferred to the goniometer head of a Bruker D8 diffractometer equipped with a PHOTON 100 detector on beamline 11.3.1 at the Advanced Light Source in Berkeley National Laboratory. Diffraction data were collected in synchrotron radiation, monochromated using silicon(111) to a wavelength of 0.7749(1) Å. A total of 68042 reflections were collected, of which 9549 were unique (R_{int} = 0.0587) and 6130 were observed [$I > 2\sigma(I)$]. The structure was solved by intrinsic phasing and refined by full-matrix least-squares on F^2 (SHELXL-2014/7)[22] using 814 parameters and 1837 restraints.

The structure of the {Ni_{18}} complex suffers from a large amount of disorder. The nickel-peroxide core is the only ordered region in this cluster. The bridging azides were found to have incongruous thermal parameters, and were modeled as disordered, sharing a site with bridging hydroxides. The hydrogen atoms on these hydroxides were not found in the difference map, so they were not refined. The organic ligand mpm$^-$ was also found to be only present at a fraction of 0.59. In its place, a nitrate is present, which is accompanied by a local azide being replaced with one of the previously mentioned bridging hydroxides, which in this case seems to donate its hydrogen to the nitrate as a hydrogen bond acceptor. The pyridyl bond position of the ligand, when vacated, is occupied by an acetonitrile. This predicament of having a semi-present ligand has other knock-on effects; a number of azides shift and split, as well as another nitrate position appearing. There are numerous cases of large ADPs, and in two cases, they do not respond well to restraint. Further chemical knowledge would not be gained by splitting a half-occupied nitrate, so they were left large. In cases where a disordered moiety had occupancy of less than 0.5, and looked unreasonably anisotropic, it was refined isotropically. All azides, nitrates and acetonitriles were refined restrained, due to the massive amount of disorder. The ligand, which seems chiral, was supposedly racemic, but the methyl group at the chiral center was poorly behaved. This is believed to be due to the underlying acetonitrile but could also be related to mixed occupancy of the other enantiomer. The methyl-chiral center bond was constrained to 1.54(2) Å. In the case of azide/hydroxide disorder, the bridging azide nitrogen and the hydroxide oxygen atoms were constrained to share the same position and APDs (EXYZ and EADP, respectively). In cases with nitrate/azide disorder, it was difficult to correctly restrain the ADPs, and RIGU was usually the only choice. In one case of a wildly disordered acetonitrile, a thermal parameter similarity restraint was used (SIMU). There were void water molecules as well, whose occupancies were refined, while the thermal parameters were fixed. Once the occupancies converged, they were fixed, and the thermal parameters were allowed to refine. All the occupancies that were refined with mixed disordered moieties were fixed and rounded according to their esds. The refined values with esds are: 0.59063(0.00496) became 0.59; 0.85192(0.0125) became 0.85; 0.74685(0.01098) became 0.75.

The programs used for molecular graphics were Mercury[23] and Diamond.[24] Unit cell parameters and structure solution and refinement data are listed in Table 1. Deposition number 1519257 (for **1**) (https://www.ccdc.cam.ac.uk/services/structures?id=doi:10.1002/chem.202403462) contains the supplementary crystallographic data for this paper. These data are provided free of charge by the joint Cambridge Crystallographic Data Centre and Fachinformationszentrum Karlsruhe (http://www.ccdc.cam.ac.uk/structures).

Table 1. Crystallographic data for complex **1**.

Formula	$C_{34.90}H_{55}N_{82.56}Ni_{18}O_{19.40}$
M, g mol^{-1}	2998.43
Crystal system	Triclinic
Space group	P-1
a/Å	13.7102(6)
b/Å	13.8041(6)
c/Å	16.0283(7)
α/°	80.108(3)
β/°	88.151(3)
γ/°	68.778(2)
V, Å^3	2784.2(2)
Z	1
T/K	100(2)
λ/Å[a,b]	0.7749
ρ_{calc}/g cm^{-3}	1.788
μ/mm^{-1}	3.854
Measd/independent (R_{int}) reflns	68042/9549
Obsd reflns [$I > 2\sigma(I)$]	6130
R_1[c,d]	0.0534
wR_2[c,e]	0.1744
GOF on F^2	1.050
$(\Delta\rho)_{max,min}$/e Å^{-3}	0.685, −0.800

[a] Synchrotron. [b] ALS beamline 11.3.1, 'silicon 111' monochromator. [c] $I > 2\sigma(I)$. [d] $R_1 = \Sigma(||F_o| - |F_c||)/\Sigma|F_o|$. [e] $wR_2 = [\Sigma[w(F_o^2 - F_c^2)^2]/\Sigma[w(F_o^2)^2]]^{1/2}$, $w = 1/[\sigma^2(F_o^2) + [(ap)^2 + bp]$, where $p = [\max(F_o^2, 0) + 2F_c^2]/3$.

Physical Measurements

Infrared spectra were recorded in the solid state on a Bruker FT-IR spectrometer (ALPHA's Platinum ATR single reflection) in the 4000–400 cm^{-1} range. NMR spectra were obtained on a Bruker Avance DPX-400 MHz instrument and these are referenced to the residual proton signal of the deuterated solvent for ^{1}H spectra, according to published values. Elemental analyses (C, H, and N) were performed on a Perkin-Elmer 2400 Series II Analyzer. Electrospray ionization (ESI) mass spectra (MS) were taken on a Bruker HCT Ultra mass spectrometer. Powder X-ray diffraction (p-XRD) studies of **1** were carried out on a X'Pert PRO Powder Diffractometer (PANalytical). Direct current (*dc*) and alternating current (*ac*) magnetic susceptibility studies were performed at the University of Barcelona Chemistry Department on a DSM5 Quantum Design magnetometer. Pascal's constants were used to estimate the diamagnetic correction, which were subtracted from the experimental susceptibility to give the molar paramagnetic susceptibility (χ_M).[25]

Results and Discussion

Synthetic Comments

Racemic mpmH (*rac*-mpmH) was prepared via the $NaBH_4$ reduction of 2-acetylpyridine according to literature reports.[21] The one-pot reaction of $Ni(NO_3)_2·6H_2O$, *rac*-mpmH, H_2O_2, NaN_3

and NEt_3 in a 6:3:1:12:3 ratio in MeCN gave a green solution which, upon slow evaporation at room temperature for two months, afforded green plate-like single crystals of $[Ni_{18}(O_2)_4(OH)_{3.62}(N_3)_{22.02}(NO_3)_{1.18}(rac\text{-mpm})_{1.18}(MeCN)_{12}]$ (**1**) in 5% yield (based on the total available Ni). The yields were small (4-5%) but reproducible, and the crystals were suitable for X-ray crystallography and magnetic studies. The chemical formula of **1** is charge balanced and accounts for the presence of significant crystallographic disorder between different pairs of N_3^-/OH^- and NO_3^-/mpm^- groups with different occupancies, as described in detail in the crystallographic section.

When the reactions were repeated in the absence of H_2O_2, the major product was the previously reported $\{Ni_8\}$ cluster bearing tetrazolate- and azido-bridging ligands, supported by chelating mpmH groups.[20] The tetrazolate ligands of the $\{Ni_8\}$/tetrazolate/mpmH cluster are formed from an solvent and the N_3^- ions under mild, room-temperature conditions. In contrast, the presence of peroxide ions in the reaction mixture appears to facilitate the formation of a larger in nuclearity $\{Ni_{18}\}$ nanosized cluster with a unique topology and very interesting magnetic properties. Additional alterations to the reported reaction conditions which afford **1**, have led to smaller in nuclearity products ($\{Ni_2\}$ dimers and $\{Ni_4\}$ tetramers) with well-known motifs and topologies.[19]

Structural Studies

The centrosymmetric molecular structure of **1** (Figure 1, **top**) consists of 18 Ni^{II} atoms bridged by four $\eta^3{:}\eta^3{:}\mu_6$ O_2^{2-} ions, fourteen μ_3-1,1,1 end-on bridging N_3^-/OH^- and ten μ-1,1 end-on bridging N_3^- groups, as well as two $\eta^1{:}\eta^3{:}\mu_3$ mpm^- ligands. The organic chelate was found to be present only a fraction of the time (0.59), coordinated to Ni9 and Ni9′. In its place, a NO_3^- is present, which is accompanied by a local N_3^- being replaced by a bridging OH^-. The Ni-$N_{pyridyl}$ bond, when vacated, is occupied by a terminal MeCN. All Ni^{II} atoms are six-coordinate with distorted octahedral geometries which are completed by twelve terminally bound MeCN solvate molecules. The $[Ni_{18}(\mu_6\text{-}O_2)_4(\mu_3\text{-}N_3/OH)_{14}(\mu\text{-}N_3)_{10}(\mu_3\text{-}OR)_2]^{2+}$ core topology of **1** resembles a 'flying saucer' motif comprising eight $\{Ni_4(\mu_3\text{-}X)_4\}^{4+}$ ($X^- = N_3^-$, OH^-, OR^-) edge-sharing cubane subunits (Figure 1, **bottom**). The core of **1**, when viewed along the crystallographic *a*-axis, can be alternatively described as a layered structure of $Ni_3/Ni_6/Ni_6/Ni_3$ subunits linked together through peroxido O_2^{2-} ions and bridging N_3^-/OH^- groups (Figure 2), further emphasizing the bridging versatility and flexibility of the employed 'ligand blend'. The Ni-O_2^{2-}-Ni and Ni-N_3^-/OH^--Ni angles span the range 101.7-110.0° and 94.8-110.6°, respectively, allowing for the presence of both antiferro- and ferromagnetic exchange interactions based on well-established magnetostructural correlations, *vide infra*.[14,26]

The space-filling representation (Figure 3) shows that **1** adopts a bowl-shaped conformation with a diameter of ~19 Å, defined by the longest C···C distance, excluding the H-atoms. The shortest Ni···Ni separation between neighboring $\{Ni_{18}\}$ clusters in the crystal is 6.514(1) Å. This packing arrangement is

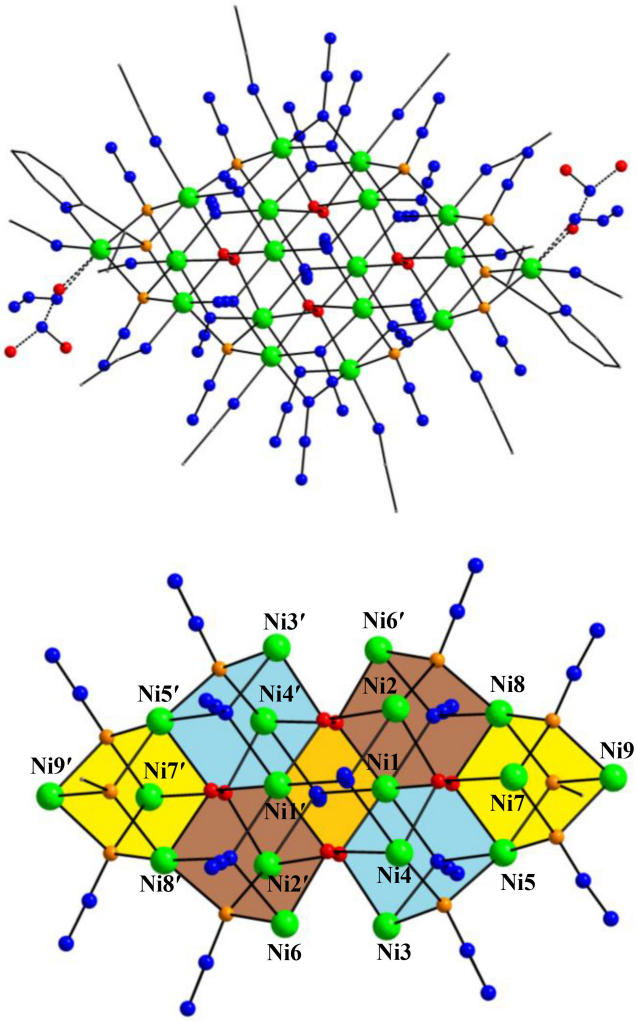

Figure 1. Structure of **1** (top) and its complete core (bottom), emphasizing with different colors the repeating $\{Ni_4\}$ cubane subunits. H atoms are omitted for clarity. Color scheme: Ni^{II} green, N blue, O red, O/N orange, C gray.

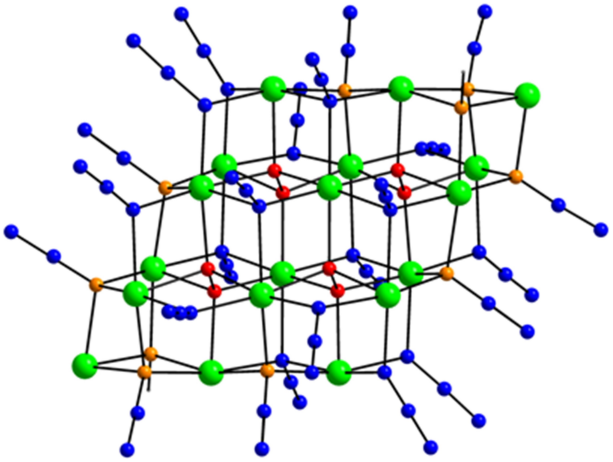

Figure 2. Different view of the layered core of **1** along the crystallographic *a*-axis. Color scheme as in Figure 1.

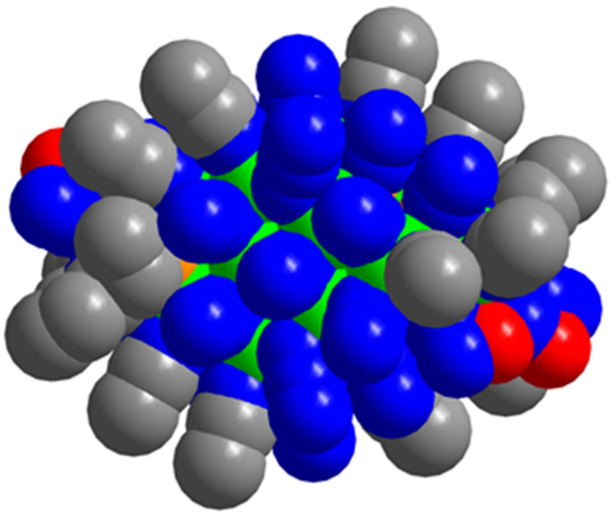

Figure 3. Space-filling representation of **1** showing its bowl-shaped conformation with a diameter of ~19 Å, defined by the longest C···C distance. Color scheme as in Figure 1.

further stabilized by the presence of weak C–H···N contacts in the range of 2.38 to 2.60 Å.

Magnetic Studies

Variable-temperature *dc* magnetic susceptibility measurements were performed on freshly-prepared, analytically-pure microcrystalline samples of **1**·2H_2O in the temperature range 2–300 K. The phase purity of the microcrystalline samples of **1** was further confirmed by p-XRD studies (Figure S4). The magnetic studies were repeated three times using three different batches of crystals of **1** and the results were reproducible. A *dc* field of 0.3 T was applied from 40 to 300 K and a weak *dc* field of 0.02 T was applied from 2 to 40 K to avoid saturation effects. The data are shown as a $\chi_M T$ *vs* *T* plot in Figure 4. The value of the $\chi_M T$ product at 300 K is 24.77 $cm^3 \cdot mol^{-1} \cdot K$, higher than the value of 21.78 $cm^3 \cdot mol^{-1} \cdot K$ (calculated with $g = 2.2$) expected for eighteen non-interacting, high-spin Ni^{II} ($S = 1$) atoms. The $\chi_M T$ product slightly increases in the 300–50 K region and then inclines faster to a value of 80.74 $cm^3 \cdot mol^{-1} \cdot K$ at 18 K, before dropping rapidly to a value of 23.68 $cm^3 \cdot mol^{-1} \cdot K$ at 2 K. The shape of the curve suggests that both ferro- and antiferromagnetic exchange interactions are likely present within **1**. The ferromagnetic interactions are most likely promoted by the end-on bridging azido and alkoxido groups, while the bridging peroxides probably favour an antiparallel alignment of the spin vectors,[26] although the exchange across the crystallographic inversion centre must be ferromagnetic in order to afford a non-zero spin ground state. The ferromagnetic component appears to dominate until ~18 K, stabilizing spin states with large *S* values, whereas at $T < 18$ K the antiferromagnetic contribution gives rise to the population of smaller, but still appreciable non-zero spin states.

Magnetization (*M*) *vs* applied field (*H*) measurements at 2 K show a continuous increase of *M* with increasing field (inset of Figure 4), reaching an unsaturated value of 18.4 $N\mu_B$ at the maximum applied field of 5 T. Reduced magnetization studies (Figure 5) indicate a strong anisotropy but attempts to fit the experimental data were unsuccessful, assuming that only one well-isolated ground state is populated. The data are consistent with a strongly anisotropic formal ground state of *S*~10 with a large mixture of states very close in energy even at very low temperatures. Considering the anisotropic response for this moderately large spin, zero-field-cooled (ZFC) and field-cooled (FC) measurements were performed at 50 G, revealing divergent plots below 13 K (Figure S5). These suggest the presence of some degree of remnant magnetization, which agrees with the small opening of the hysteresis cycle (30 G) measured at 2 K and an SMM response (*vide infra*).

To study the slow relaxation of the magnetization for **1**, alternating current (*ac*) magnetic susceptibility studies in zero static *dc* field were performed in the 2–26 K temperature range

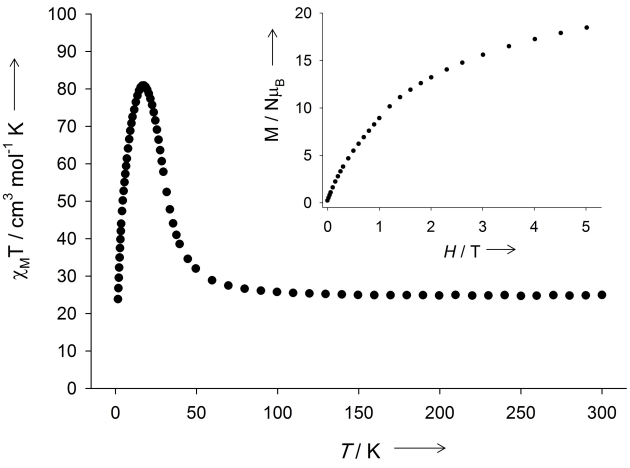

Figure 4. $\chi_M T$ *vs* *T* plot for **1**·2H_2O. (inset) Magnetization (*M*) *vs* field (*H*) plot for **1**·2H_2O at 2 K.

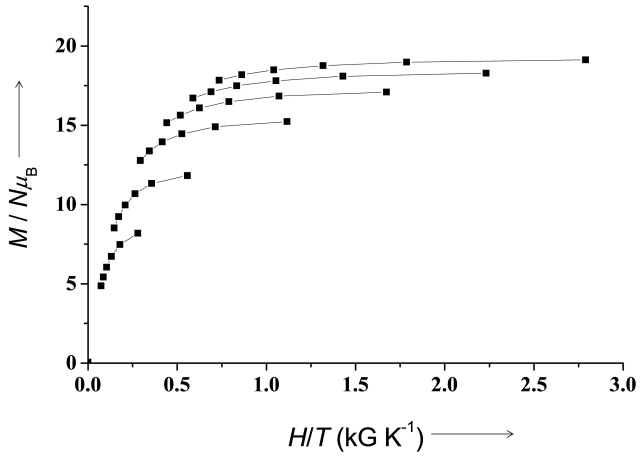

Figure 5. Plot of reduced magnetization ($M/N\mu_B$) *vs* H/T for **1**·2H_2O in the temperature range 1.8-6.8 K and in the field range 0–5 T. Solid lines are guides for the eye only. The various isofield lines are not superimposed, thus indicating the presence of significant magnetic anisotropy and low-lying excited states.

using a 4.0 G *ac* field oscillating at frequencies from 1.0 to 1488 Hz. The in-phase (χ'_M) and out-of-phase (χ''_M) signals are frequency and temperature-dependent (Figures 6 and S6), showing well-defined peaks in the temperature range ~10–24 K and weak tails of signals below ~5 K. The data were re-arranged

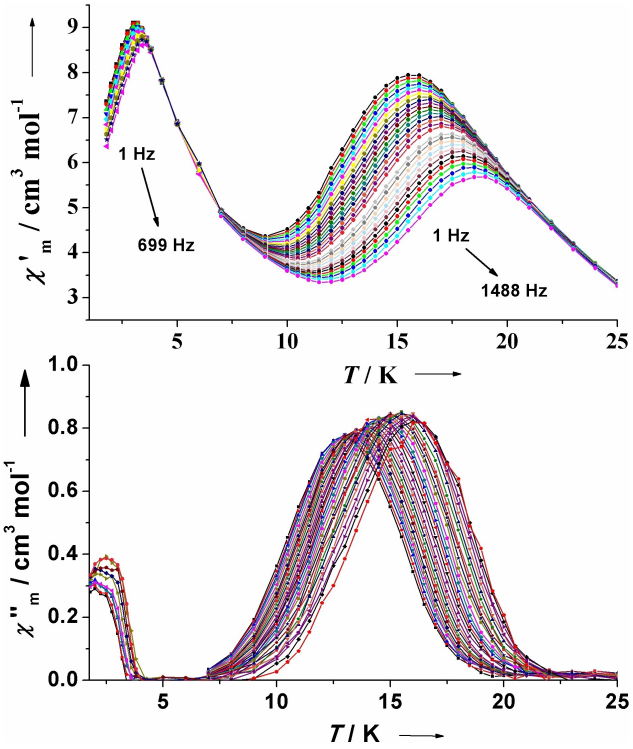

Figure 6. In-phase (χ'_M, top) and out-of-phase (χ''_M, bottom) *vs T ac* susceptibility signals for **1** in zero static *dc* field, with a 4.0 G *ac* field oscillating at the indicated frequencies. The data used at the low-*T* regime are for frequencies in the range 1–699 Hz due to the noisy signals at higher frequencies. The solid lines are guides only.

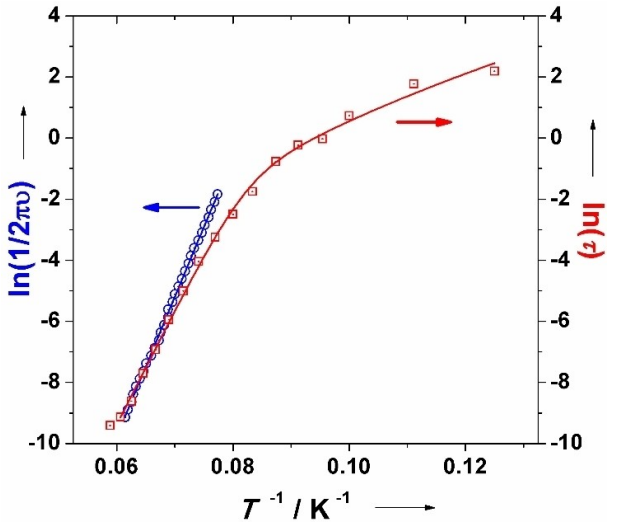

Figure 7. Right axis: ln(τ) *vs* 1/*T* data from the fit of the Argand plots (red squares, temperature range: 10–20 K). Left axis: Arrhenius plot constructed from the peak maxima located at the high temperature regime (blue circles, temperature range: 13–16.2 K). Solid lines represent the best-fit of the experimental data.

in the form of χ''_M *vs* χ'_M plots (Argand plots, Figure S7) and fitted using the generalized Debye model *via* the CC-FIT software to extract the relaxation times (τ) at each temperature.[27,28] From the log-log plot of τ *vs T* (Figure S8), it becomes apparent that there are two distinct slopes, each dominated at a particular temperature range, which corroborates the presence of two independent relaxation processes.

The relaxation data were further represented in the form of an Arrhenius plot as ln(τ) *vs* 1/*T* (Figure 7). The data in the 10–20 K temperature range were fitted accounting for the Raman (CT^n) and Orbach relaxation pathways, according to the expression:

$$\tau^{-1} = CT^n + \tau_0^{-1} \cdot \exp(-U_{eff}/k_B T)$$

The best-fit parameters were: $U_{eff} = 261(9)$ K, $\tau_0 = 1.4(8) \times 10^{-13}$ s and a Raman coefficient, *C*, of 8.50(6). In order to avoid over-parameterization, *n* was fixed to different values, until the best fitting coefficient was obtained. The results indicate that the major operating relaxation mechanism is through the thermally-assisted Orbach process with the co-presence of a weak Raman component. The contributions from the direct- and QTM-processes were excluded from the fitting model as these relaxation mechanisms should only be operative at lower temperatures. The predominant Orbach relaxation agrees with the Arrhenius-type plot constructed from the χ''_M *vs T* maxima found between 12.5-16 K in the high-temperature regime (Figure 7), which gives an effective energy barrier (U_{eff}) of 381.3 K and $\tau_0 = 2.7 \times 10^{-15}$ s, where τ_0 is the pre-exponential factor. The small value of τ_0 is not uncommon in large *3d*-clusters and is likely due to the presence of intermolecular interactions between the cluster units in the crystal, several types of disorder in the molecular and crystal lattice environments, and/or low-lying excited states.[29] Moreover, the shift (ΔT_{max}) in the χ''_M peak maximum temperature (T_{max}) with *ac* frequency (*f*) was measured by a parameter φ, where $\varphi = (\Delta T_{max}/T_{max})/\Delta(\log f)$. For **1** we obtained $\varphi = 0.07$-0.10, which is within the range of normal superparamagnets, thereby excluding the possibility of a spin glass state.[30]

To examine the additional low-temperature SMM behavior of **1**, detailed magnetization (*M*) *vs dc* field studies were undertaken to look for hysteresis, the diagnostic property of a magnet. The data were collected on single-crystals of **1** that had been kept in contact with mother liquor using a micro-SQUID apparatus. Hysteresis loops were indeed observed below ~1.3 K, whose coercivities increase with decreasing temperature and increasing field sweep rate (Figure 8), as expected for the superparamagnetic-like properties of a SMM below its blocking temperature. The loops do not show the steps characteristic of QTM, as expected for large SMMs since they are more susceptible to various step-broadening effects from low lying excited states, intermolecular interactions, and distributions of local environments owing to ligand and solvent disorder.

For relaxation rate *vs T* data in the low temperature regime where no peaks of *ac* signals were observed, the crystal's magnetization was first saturated in one direction at ~5 K with a large applied *dc* field, the temperature decreased to a chosen

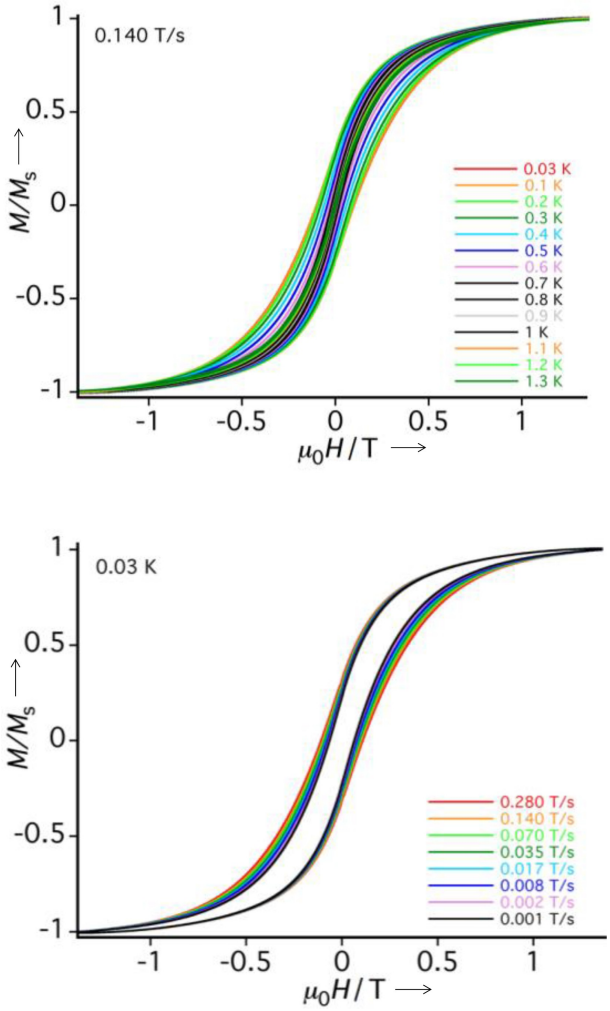

Figure 8. Magnetization (*M*) *vs* applied *dc* field ($\mu_0 H$) hysteresis loops for a single crystal of **1** at the indicated temperatures (top) and field sweep rates (bottom). The magnetization is normalized to its saturation value (M_s).

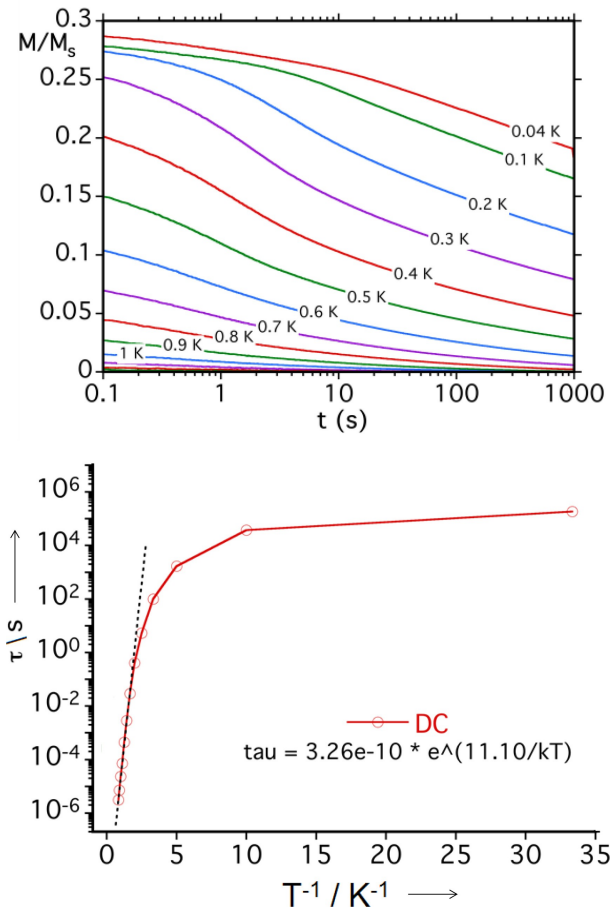

Figure 9. (top) Magnetization (*M*) *vs* time decay plots in zero *dc* field for a single-crystal of **1**. The magnetization is normalized to its saturation value (M_s). (bottom) Arrhenius plot of the relaxation time (τ) *vs* T^{-1} for a single crystal of **1** using data obtained from the *dc* magnetization decay measurements at the low temperature regime. The dashed line is the fit of data in the thermally-activated region to the Arrhenius equation; see the text and inset for the fit parameters.

value in the 0.04-1.3 K range, and then the field was removed and the magnetization decay monitored with time (Figure 9, **top**). The resulting relaxation rate ($1/\tau$) *vs* *T* data were then used to construct an Arrhenius plot, as shown in Figure 9 (**bottom**). The fit to the thermally-activated region gave $\tau_0 = 3.26\times10^{-10}$ s and $U_{eff} = 11.10$ K. At ~0.1 K and below, the relaxation becomes temperature-independent, consistent with relaxation via ground state QTM.

The observation of relaxation processes in two different temperature regimes in this $\{Ni_{18}\}$ cluster is very rare for *3d*-metal based SMMs and to the best of our knowledge, has only been previously observed for a few members of the $\{Mn_{12}\}$ family of SMMs as a result of the 'Jahn-Teller isomerism' effect.[31] Moreover, few of us, recently reported a rare "Janus"-faced $\{Fe^{II}_7\}$-azido SMM exhibiting intramolecular ferromagnetic interactions and two relaxation processes at two different temperature regimes due to solvation effects in the coordination sphere of the metal ions.[32] In the case of **1**, our rationalization relies mainly on the effect of the spin, *S*, on the magnitude of *U* at different temperatures. Therefore, it is very likely that the large barrier obtained in the high-*T* regime results from a large value of *S* (or mixture of states with large *S*), in contrast to the usual low-*T* relaxation for Ni^{II} SMMs which arises from spin states with smaller *S* values. Currently, there is no estimate of the value of *D* and its effect on the anisotropy barrier; further studies, including single-crystal HFEPR measurements and inelastic neutron scattering, will hopefully shed more light on the origin of the relaxation and the effects of *S* and *D* on the magnitude of the energy barrier(s). These results will be reported in due course.[33]

Conclusions

In conclusion, we have reported a new $\{Ni_{18}\}$ cluster **1**, assembled from α-methyl-2-pyridine-methanol in conjunction with azido (N_3^-) and peroxide (O_2^{2-}) ligands. The nanosized complex **1** represents one of the highest nuclearity Ni^{II} clusters reported to date and possesses a unique structural topology resembling a 'flying saucer'. Magnetic studies revealed a very

rare SMM profile for **1**, with two relaxation processes occurring at lower- and higher-temperature ranges, as documented by the presence of frequency-dependent out-of-phase *ac* signals at ~15 K and molecular magnetic hysteresis (on single-crystals of **1**) at ~1.3 K. Our findings demonstrate that *3d*-metal cluster based SMMs are capable of bridging the gap between traditional nanoscale and molecular/quantum magnetic materials. This in turn may serve to re-kindle interest in the discovery of SMMs with high energy barriers derived from polynuclear *3d*-metal clusters *via* the development of new synthetic approaches that involve the use of benign metals together with unexplored 'ligand blends'.

Supporting Information

Additional spectroscopic and magnetism data and plots supporting this article have been included as part of the ESI.

Acknowledgements

This work was supported by Brock University (Chancellor's Chair for Research Excellence, Th.C.S), Tier II CRC (M.P), NSERC-DG (DG-2018-04255 to M.P), ERA (Th.C.S), CFI (M.P) and OTS (P.A). A.E acknowledges financial support from Ministerio de Economía y Competitividad, Project PID2023-146166NB-I00. The Advanced Light Source is supported by the Director, Office of Science, Office of Basic Energy Sciences, of the U.S. Department of Energy under Contract No. DE-AC02-05CH11231. C.M.B is supported by COMPRES, the Consortium for Materials Properties Research in Earth Sciences under NSF Cooperative Agreement EAR 11–57758.

Conflict of Interests

The authors declare no conflict of interest.

Data Availability Statement

The data that support the findings of this study are available in the supplementary material of this article.

Keywords: nickel · coordination clusters · structural chemistry · relaxation of magnetization · single-molecule magnets

[1] For example, see: a) D. Gatteschi, R. Sessoli, J. Villain, in *Molecular Nanomagnets*, Oxford University Press, Oxford, **2006**; b) D. Gatteschi, R. Sessoli, *Angew. Chem. Int. Ed.* **2003**, *42*, 268–297; c) G. Aromi, E. K. Brechin, *Struct. Bonding (Berlin)* **2006**, *122*, 1–69.
[2] a) R. Sessoli, A. K. Powell, *Coord. Chem. Rev.* **2009**, *253*, 2328–2341; b) R. Bagai, G. Christou, *Chem. Soc. Rev.* **2009**, *38*, 1011–1026.
[3] a) W. Wernsdorfer, R. Sessoli, *Science* **1999**, *284*, 133–135; b) W. Wernsdorfer, N. Aliaga-Alcalde, D. N. Hendrickson, G. Christou, *Nature* **2002**, *416*, 406–409; c) S. Hill, R. S. Edwards, N. Aliaga-Alcalde, G. Christou, *Science* **2003**, *302*, 1015–1018.
[4] R. Sessoli, H. L. Tsai, A. R. Schake, S. Wang, J. B. Vincent, K. Folting, D. Gatteschi, G. Christou, D. N. Hendrickson, *J. Am. Chem. Soc.* **1993**, *115*, 1804–1816.
[5] a) C. Papatriantafyllopoulou, E. E. Moushi, G. Christou, A. J. Tasiopoulos, *Chem. Soc. Rev.* **2016**, *45*, 1597–1628; b) R. Inglis, C. J. Milios, L. F. Jones, S. Piligkos, E. K. Brechin, *Chem. Commun.* **2012**, *48*, 181–190.
[6] A. A. Athanasopoulou, M. Pilkington, C. P. Raptopoulou, A. Escuer, Th. C. Stamatatos, *Chem. Commun.* **2014**, *95*, 14942–14945.
[7] a) L. Bogani, W. Wernsdorfer, *Nat. Mater.* **2008**, *7*, 179–186; b) G. A. Craig, M. Murrie, *Chem. Soc. Rev.* **2015**, *44*, 2135–2147; c) J. M. Frost, K. L. M. Harriman, M. Murugesu, *Chem. Sci.* **2016**, *7*, 2470–2491.
[8] C. J. Milios, A. Vinslava, W. Wernsdorfer, S. Moggach, S. Parsons, S. P. Perlepes, G. Christou, E. K. Brechin, *J. Am. Chem. Soc.* **2007**, *129*, 2754–2755.
[9] a) C. J. Milios, R. E. P. Winpenny, *Struct. Bonding (Berlin)* **2015**, *164*, 1–109; b) P. Happ, C. Plenk, E. Rentschler, *Coord. Chem. Rev.* **2015**, *289*, 238–260.
[10] N. Ishikawa, M. Sugita, T. Ishikawa, S. Koshihara, Y. Kaizu, *J. Am. Chem. Soc.* **2003**, *125*, 8694–8695.
[11] For example, see: a) N. D. Woodruff, R. E. P. Winpenny, R. A. Layfield, *Chem. Rev.* **2013**, *113*, 5110–5148; b) J. D. Rinehart, J. R. Long, *Chem. Sci.* **2011**, *2*, 2078–2085; c) P. Zhang, Y.-N. Guo, J. Tang, *Coord. Chem. Rev.* **2013**, *257*, 1728–1763.
[12] a) R. A. Layfield, M. Murugesu, in *Lanthanides and Actinides in Molecular Magnetism*, Wiley, **2015**; b) E. L. Gavey, Y. Beldjoudi, J. M. Rawson, Th. C. Stamatatos, M. Pilkington, *Chem. Commun.* **2014**, *50*, 3741–3743.
[13] a) A. J. Tasiopoulos, S. P. Perlepes, *Dalton Trans.* **2008**, 5537–5555; b) Th. C. Stamatatos, K. A. Abboud, W. Wernsdorfer, G. Christou, *Angew. Chem. Int. Ed.* **2007**, *46*, 884–888; c) Th. C. Stamatatos, K. A. Abboud, W. Wernsdorfer, G. Christou, *Angew. Chem. Int. Ed.* **2006**, *45*, 4134–4137.
[14] For a review, see: A. Escuer, J. Esteban, S. P. Perlepes, Th. C. Stamatatos, *Coord. Chem. Rev.* **2014**, *275*, 87–129.
[15] E.-C. Yang, W. Wernsdorfer, L. N. Zakharov, Y. Karaki, A. Yamaguchi, R. M. Isidro, G.-D. Lu, S. A. Wilson, A. L. Rheingold, H. Ishimoto, D. N. Hendrickson, *Inorg. Chem.* **2006**, *45*, 529–546.
[16] a) R. Boča, *Coord. Chem. Rev.* **2004**, *248*, 757–815; b) C. Cadiou, M. Murrie, C. Pailsen, V. Villar, W. Wernsdorfer, R. E. P. Winpenny, *Chem. Commun.* **2001**, 2666–2667; c) M. Moragues-Canova, M. Helliwell, L. Ricard, E. Riviere, W. Wernsdorfer, E. K. Brechin, T. Mallah, *Eur. J. Inorg. Chem.* **2004**, 2219–2222; d) S. T. Ochsenbein, M. Murrie, E. Rusanov, H. Stoeckli-Evans, C. Sekine, H. U. Güdel, *Inorg. Chem.* **2002**, *41*, 5133; e) G. Aromí, E. Bouwman, E. Burzurí, C. Carbonera, J. Krzystek, F. Luis, C. Schlegel, J. van Slageren, S. Tanase, S. J. Teat, *Chem. Eur. J.* **2008**, *14*, 11158–11166; f) G. Aromí, S. Parsons, W. Wernsdorfer, E. K. Brechin, E. J. L. McInnes, *Chem. Commun.* **2005**, 5038–5040.
[17] A. Trinh Pham, P. Abbasi, G. Delle Monache, E. C. Mazarakioti, J. M. Rawson, Th. C. Stamatatos, M. Pilkington, *Polyhedron* **2019**, *170*, 34–40.
[18] P. Abbasi, K. Quinn, D. I. Alexandropoulos, M. Damjanović, W. Wernsdorfer, A. Escuer, J. Mayans, M. Pilkington, Th. C. Stamatatos, *J. Am. Chem. Soc.* **2017**, *139*, 15644–15647.
[19] J. Mayans, A. A. Athanasopoulou, A. Trinh Pham, M. Font-Bardia, E. C. Mazarakioti, M. Pilkington, Th. C. Stamatatos, A. Escuer, *Dalton Trans.* **2019**, *48*, 10427–10434.
[20] P. Abbasi, A. A. Athanasopoulou, E. C. Mazarakioti, K. J. Gagnon, S. J. Teat, A. Escuer, M. Pilkington, Th. C. Stamatatos, *Dalton Trans.* **2019**, *48*, 11632–11636.
[21] M. Kamitani, M. Ito, M. Itazaki, H. Nakazawa, *Chem. Commun.* **2014**, *50*, 7941–7944.
[22] G. M. Sheldrick, *Acra Cryst.* **2008**, *A64*, 112–122.
[23] Mercury, I. J. Bruno, J. C. Cole, P. Edgington, M. K. Kessler, C. F. Macrae, P. McCabe, J. Pearson, R. Taylor, *Acta Crystallogr. Sect. B* **2002**, *58*, 389–397.
[24] K. Bradenburg, *DIAMOND, Release 3.1f, Crystal Impact GbR*; Bonn, Germany, **2008**.
[25] G. A. Bain, J. F. Berry, *J. Chem. Educ.* **2008**, *85*, 532–536.
[26] For examples of Ni/O_2^{2-}-bridged complexes, see: a) A. Perivolaris, C. C. Stoumpos, J. Karpinska, A. G. Ryder, J. M. Frost, K. Mason, A. Prescimone, A. M. Z. Slawin, V. G. Kessler, J. S. Mathieson, L. Cronin, E. K. Brechin, G. S. Papaefstathiou, *Inorg. Chem. Front.* **2014**, *1*, 487–494; b) E. J. Brown, A.-K. Duhme-Klair, M. I. Elliott, J. E. Thomas-Oates, P. L. Timmins, P. H. Walton, *Angew. Chem. Int. Ed.* **2005**, *44*, 1392–1395.
[27] a) P. Debye, *Phys. Z.* **1938**, *39*, 616–618; b) K. S. Cole, R. H. Cole, *J. Chem. Phys.* **1941**, *9*, 341–351.
[28] D. Reta, N. F. Chilton, *Phys. Chem. Chem. Phys.* **2019**, *21*, 23567– 23575.

[29] For example, see: a) E. E. Moushi, Th. C. Stamatatos, W. Wernsdorfer, V. Nastopoulos, G. Christou, A. J. Tasiopoulos, *Inorg. Chem.* **2009**, *48*, 5049–5051; b) Th. C. Stamatatos, D. Foguet-Albiol, W. Wernsdorfer, K. A. Abboud, G. Christou, *Chem. Commun.* **2011**, *47*, 274–276; c) M. Murugesu, S. Takahashi, A. Wilson, K. A. Abboud, W. Wernsdorfer, S. Hill, G. Christou, *Inorg. Chem.* **2008**, *47*, 9459–9470; d) E. E. Moushi, C. Lampropoulos, W. Wernsdorfer, V. Nastopoulos, G. Christou, A. J. Tasiopoulos, *J. Am. Chem. Soc.* **2010**, *132*, 16146–16155.
[30] J. A. Mydosh, *Spin Glasses: An Experimental Introduction*, Taylor & Francis, London, **1993**.
[31] a) Z. Sun, D. Ruiz, N. R. Dilley, M. Soler, J. Ribas, K. Folting, M. B. Maple, G. Christou, D. N. Hendrickson, *Chem. Commun.* **1999**, 1973–1974; b) A. J. Tasiopoulos, W. Wernsdorfer, K. A. Abboud, G. Christou, *Angew. Chem. Int. Ed.* **2004**, *43*, 6338–6342.
[32] D. I. Alexandropoulos, K. R. Vignesh, Th. C. Stamatatos, K. R. Dunbar, *Chem. Sci.* **2019**, *10*, 1626–1633.
[33] For further information about the coordination chemistry of mpmH, see: P. Abbasi, "Investigating the Cluster Chemistry of α-Methyl-2-pyridine methanol (mpmH) with Select 3d Ions", Ph.D. Thesis, Brock University, Ontario, Canada, **2020**.

Manuscript received: September 17, 2024
Accepted manuscript online: November 13, 2024
Version of record online: ■■, ■■

RESEARCH ARTICLE

A high-nuclearity $\{Ni_{18}\}$ nanosized complex with an unprecedented 'flying saucer' motif has been prepared from the organic chelate α-methyl-2-pyridine-methanol (mpmH) in conjunction with bridging azido and peroxido groups. The $\{Ni_{18}\}$ compound behaves as single-molecule magnet and exhibits very rare two relaxation processes at 15 and 1.3 K.

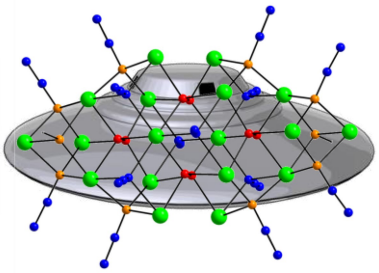

Dr. A. A. Athanasopoulou, Dr. P. Abbasi, Dr. D. I. Alexandropoulos, Dr. J. J. Hayward, Dr. C. M. Beavers, Dr. S. J. Teat, Prof. Dr. W. Wernsdorfer, Dr. J. Mayans, Prof. Dr. A. Escuer, Prof. Dr. M. Pilkington, Prof. Dr. T. C. Stamatatos**

1 – 10

A Nanosized $\{Ni^{II}_{18}\}$ Cluster with a 'Flying Saucer' Topology Exhibiting Slow Relaxation of Magnetisation Phenomena at Both 15 K and 1.3 K